Motor Domain Mutation Traps Kinesin as a Microtubule Rigor Complex †

ARTICLE *in* BIOCHEMISTRY · APRIL 2003

Impact Factor: 3.02 · DOI: 10.1021/bi026715r · Source: PubMed

Motor Domain Mutation Traps Kinesin as a Microtubule Rigor Complex†

Lisa M. Klumpp,‡ Katherine M. Brendza,§,|| John M. Rosenberg,‡ Andreas Hoenger,⊥ and Susan P. Gilbert*,‡

Department of Biological Sciences, University of Pittsburgh, Pittsburgh, Pennsylvania 15260, Department of Biology, Indiana University, Bloomington, Indiana 47405, and European Molecular Biology Laboratory, Meyerhofstrasse 1, D-69012 Heidelberg, Germany

Received August 23, 2002; Revised Manuscript Received January 14, 2003

ABSTRACT: Conventional kinesin is a highly processive, microtubule-based motor protein that drives the movement of membranous organelles in neurons. Using in vivo genetics in *Drosophila melanogaster*, Glu^{164} was identified as an amino acid critical for kinesin function [Brendza, K. M., Rose, D. J., Gilbert, S. P., and Saxton, W. M. (1999) *J. Biol. Chem. 274*, 31506−31514]. Glu^{164} is located at the β-strand 5a/loop 8b junction of the catalytic core and projects toward the microtubule binding face in close proximity to key residues on β-tubulin helix α12. Substitution of Glu^{164} with alanine (E164A) results in a dimeric kinesin with a dramatic reduction in the microtubule-activated steady-state ATPase (5 s^{-1} per site versus 22 s^{-1} per site for wild-type). Our analysis shows that E164A binds ATP and microtubules with a higher affinity than wild-type kinesin. The rapid quench and stopped-flow results provide evidence that ATP hydrolysis is significantly faster and the precise coordination between the motor domains is disrupted. The data reveal an E164A intermediate that is stalled on the microtubule and cannot bind and hydrolyze ATP at the second head.

Conventional kinesin is a processive, dimeric microtubule motor protein that travels toward the plus end of the microtubule in 8 nm steps (reviewed in refs *1*−*5*). The processive steps require coordination between the two motor domains and with the microtubule, which is achieved through the ATPase cycle (*6*−*13*). The amino acid sequence of the nucleotide binding motifs and the crystal structure of the catalytic core show homology with other kinesin superfamily members, myosins, and G proteins (P-loop nucleotidases). These results suggest a common mechanism through switch I and switch II that translates the state of the nucleotide bound at the catalytic core into structural transitions to communicate with protein partners (*14*−*23*; reviewed in refs *24*−*27*).

C-Terminal to the catalytic core of kinesin is the neck region, which consists of two short β strands (neck linker) followed by a coiled-coil helix (neck coiled-coil) (*16*). The neck linker controls the plus-end directionality of kinesin movement (*20*, *28*−*31*). In addition, crystal structures of dimeric kinesin and Ncd docked on the microtubule by cryo-EM[1] reconstruction (*16*, *20*, *32*−*37*) show specific neck linker conformations for the plus-end and minus-end directed dimeric motors and position them differently on the microtubule. The kinesin neck linker interacts with the catalytic core near microtubule binding loop L12 and the switch II relay helix, α4, which is involved in the communication between the nucleotide and microtubule binding sites (*31*, *38*).

Rice et al. (*31*) showed for a kinesin monomer that ATP promoted neck linker docking onto the catalytic core and the orientation was toward the plus end of the microtubule. ATP hydrolysis resulted in the neck linker returning to a more mobile conformation. On the basis of these results, Rice et al. proposed that the energy from ATP binding is coupled to neck linker docking onto the catalytic core. They suggested that the structural transition leads to a plus-end directed swing of the neck linker to position the partner motor domain forward onto the next microtubule binding site 16 nm away from its present position. The forward head would be in a nucleotide state in which the neck linker is mobile and therefore undocked, while the rearward head is docked onto the catalytic core, thus allowing for both motor domains to be microtubule bound yet separated by 8 nm.

These results with monomeric kinesin viewed within the context of an alternating site mechanism of ATP hydrolysis, mechanical data showing a load-dependent ATP state, and recent structural studies provide a plausible model for force generation (*6*, *8*, *9*, *11*, *13*, *35*, *39*−*42*). Kinetic analysis of kinesin switch I mutants has further defined the role of ATP hydrolysis for motor domain coordination. Farrell et al.

† This work was supported by Grant GM54141 from the National Institute of General Medical Sciences and through Career Development Award K02-AR47841 from the National Institute of Arthritis and Musculoskeletal and Skin Diseases, National Institute of Health, Department of Health and Human Services.

* Corresponding author. Tel: (412) 624-5842. Fax: (412) 624-4759. E-mail: spg1@pitt.edu.

‡ University of Pittsburgh.

§ Indiana University.

|| Present address: Department of Biochemistry and Molecular Biophysics, Washington University School of Medicine, St. Louis, MO 63110.

⊥ European Molecular Biology Laboratory.

[1] Abbreviations: EM, electron microscopy; K401, *Drosophila* kinesin heavy chain construct containing the N-terminal 401 amino acids; E164A, mutant kinesin motor K401 with alanine substituted for glutamate at amino acid residue 164; K401-wt, wild-type K401; Mt, microtubule; Mt·K401, microtubule−K401 complex; mantATP, 2′(3′)-*O*-(*N*-methylanthraniloyl)adenosine 5′-triphosphate; mantADP, 2′(3′)-*O*-(*N*-methylanthraniloyl)adenosine 5′-diphosphate; P_i, inorganic phosphate.

10.1021/bi026715r CCC: $25.00
Published on Web 02/14/2003

proposed that ATP hydrolysis is required on the first head to lock the second head onto the microtubule before the first head can dissociate from the microtubule (*43*). This mechanism of cooperativity optimizes forward movement and processivity by ensuring that one motor domain is tightly bound to the microtubule before the second one can detach.

Recently, there has been a strong interest to understand the mechanism by which tight coupling of the ATPase cycle is controlled through transition states and the structural requirements important for ATP hydrolysis, motor coordination, and processive movement along the microtubule. Analysis of kinesin mutant motors is advantageous in that they may reveal an understanding of the steps in the cross-bridge cycle that are inaccessible by studying wild-type kinesin or trap intermediates that normally are too transient to identify and study. Previously, E164K was isolated in a genetic screen for recessive lethal mutations in *Drosophila melanogaster* that disrupted axonal transport and caused lethality (*44*). The residue Glu^{164} is identical in the KHC subfamily, conserved in the superfamily, and located on the boundary of β-strand 5a and loop 8b on the surface of the motor. The steady-state analysis of this mutant showed that although Glu^{164} is distant from the active site, the lysine substitution caused critical defects in the ATPase cycle of kinesin. We report here that E164A shows distinct kinetic defects in its ATPase cycle, and these result in a kinesin intermediate that is stalled on the microtubule, unable to bind and hydrolyze ATP at its second motor domain.

EXPERIMENTAL PROCEDURES

Materials. [α-^{32}P]ATP (>3000 Ci/mmol) was from NEN Life Sciences (Boston, MA), polyethylenimine (PEI)−cellulose TLC plates (EM Science of Merck, 20 × 20 cm, plastic backed) were from VWR Scientific (Bridgeport, NJ), Paclitaxel (taxol, *Taxus brevifolia*) was from Calbiochem-Novabiochem International (San Diego, CA), the Chameleon double-stranded site-directed mutagenesis kit was from Statagene, Inc. (La Jolla, CA), ATP, GTP, and S-Sepharose were from Amersham Pharmacia Biotech (Uppsala, Sweden), and Bio-Rad protein assay, ovalbumin, IgG, and DEAE-Sephacel were from Bio-Rad (Hercules, CA).

Expression and Purification of Kinesin Mutant E164A. The kinesin mutant, E164A, was constructed by introducing a single amino acid change in the K401-wt plasmid, pET5b-K401 (*45*), using the Chameleon double-stranded site-directed mutagenesis protocol (Stratagene, Inc., La Jolla, CA). DNA sequencing verified the glutamate to alanine substitution at residue 164, and the protein was expressed in *Escherichia coli* BL21(DE3)pLysS. The mechanistic behavior of E164A was directly compared to K401-wt, a dimeric kinesin motor that has been well characterized (*6*, *7*, *11*, *44*−*48*). The concentration of E164A was determined using the Bio-Rad protein assay with IgG as a protein standard. The E164A protein was purified to >95% homogeneity and >95% activity on the basis of active site titration (*49*). Throughout this paper, K401-wt and E164A concentrations are expressed as the concentration of ATP binding sites although both proteins are dimeric.

Taxol-Stabilized Microtubules. Purified bovine brain tubulin was cold-depolymerized and clarified prior to polymerization the morning of each experiment. The concentrations of tubulin reported reflect the tubulin assembled into microtubules and stabilized with 20 μM taxol.

Experimental Conditions. All experiments reported were performed in ATPase buffer (20 mM HEPES, pH 7.2, with KOH, 5 mM magnesium acetate, 0.1 mM EGTA, 0.1 mM EDTA, 50 mM potassium acetate, and 1 mM DTT) at 25 °C. The concentrations reported are the final concentrations after mixing.

Steady-State ATPase Assays. ATPase assays were performed at 22−25 °C in ATPase buffer at 50 mM potassium acetate by following the hydrolysis of [α-^{32}P]ATP as described previously (*45*). All concentrations reported are final after mixing. The steady-state ATPase measurements as a function of ATP concentration (Figure 2A) were fit to a hyperbola to determine the $k_{cat,ATP}$ and the $K_{m,ATP}$. The microtubule concentration dependence (Figure 2B) required the data be fit to the quadratic equation (eq 1) because some of the tubulin concentrations were as low as the enzyme concentration:

$$\text{rate} = 0.5k_{cat}\{(E_0 + K_{0.5,Mt} + Mt_0) - [(E_0 + K_{0.5,Mt} + Mt_0)^2 - (4E_0Mt_0)]^{1/2}\} \quad (1)$$

where rate is the amount of product formed per second per site, k_{cat} is the maximum rate constant of steady-state ATP turnover, $E_0 = 0.5$ μM kinesin, Mt_0 is the tubulin concentration, and $K_{0.5,Mt}$ is the concentration of tubulin required to provide one-half of the maximal velocity.

Active Site Experiment. Active site experiments (Figure 3) were performed as described in Gilbert and Mackey (*49*) where 5 μM E164A was incubated with trace amounts of [α-^{32}P]ATP for 0−90 min in the absence of microtubules. The experimental design assumes that kinesin motor domains that are active retain ADP tightly bound at the nucleotide binding site. During the incubation, the tightly bound ADP is released, and radiolabeled ATP binds and is hydrolyzed to [α-^{32}P]ADP + P_i. The products, [α-^{32}P]ADP + P_i, were separated from [α-^{32}P]ATP by thin-layer chromatography, and [α-^{32}P]ADP and [α-^{32}P]ATP were quantified. The concentration of [α-^{32}P]ADP was plotted as a function of time and fit to a single-exponential function. The amplitude of the single-exponential function detects the fraction of kinesin sites that are competent to bind and hydrolyze [α-^{32}P]-ATP in the absence of microtubules.

Stopped-Flow Experiments. The pre-steady-state kinetics of mantATP binding, mantADP release, microtubule association, and Mt·E164A dissociation were measured using a KinTek stopped-flow instrument (SF-2001; KinTek Corp., Austin, TX) at 25 °C in ATPase buffer. *N*-Methylanthraniloyl fluorescence (mantATP or mantADP) was excited at 360 nm and detected after being passed through a 400 nm cutoff filter. MantATP binding data in Figure 4B were fit to a linear function:

$$k_{obs} = k_{+1}[\text{mantATP}] + k_{-1} \quad (2)$$

where k_{obs} is the rate constant obtained from the exponential phase of the fluorescence enhancement, k_{+1} defines the second-order rate constant for mantATP binding, and k_{-1} corresponds to the observed rate constant of mantATP dissociation as determined by the *y*-intercept.

The dissociation kinetics of the Mt·E164A complex (Figure 8) and E164A microtubule association kinetics (Figure 9) were determined by the change in turbidity monitored at 340 nm. For Figure 9B, the observed rate constants of microtubule association were fit to the equation:

$$k_{obs} = k_{+5}[\text{tubulin}] + k_{-5} \quad (3)$$

where k_{obs} is the rate of the initial exponential phase, k_{+5} defines the second-order rate constant for microtubule association, and k_{-5} corresponds to the observed rate constant of motor dissociation as determined by the *y*-intercept.

Rapid Quench Experiments. The acid quench and pulse−chase pre-steady-state experiments (Figures 5−7) were performed with a chemical quench-flow instrument (RQF-3; KinTek Corp., Austin, TX) at 25 °C in ATPase buffer as described previously (*47*, *49*). For each time point, a preformed Mt·E164A complex was reacted with [α-^{32}P]ATP for times ranging from 3 to 400 ms. To measure ATP hydrolysis, the reaction mixture was quenched with 5 M formic acid and expelled from the instrument. The concentration of product ([α-^{32}P]ADP) was plotted as a function of time, and the data were fit to the burst equation:

$$\text{product} = A[1 - \exp(-k_b t)] + k_{ss} t \quad (4)$$

where A is the amplitude of the burst, representing the formation of [α-^{32}P]ADP·P_i at the active site during the first ATP turnover, k_b is the rate constant of the pre-steady-state exponential burst phase, k_{ss} is the rate constant of the linear phase and when divided by the enzyme concentration corresponds to steady-state turnover, and t is the time in seconds.

Pulse−Chase Experiments. To measure the kinetics of ATP binding and to investigate the reduced burst amplitude, pulse−chase experiments were performed such that the Mt·E164A·[α-^{32}P]ATP reaction mixture was chased with 10 mM MgATP for 0.9 s and then quenched by 5 M formic acid. The chase would allow bound [α-^{32}P]ATP to be converted to [α-^{32}P]ADP·P_i, yet any substrate unbound or bound loosely to the active site would be diluted by the excess unlabeled MgATP chase.

Equilibrium Binding Experiments. The microtubule binding experiments were performed with 2 μM enzyme incubated with taxol-stabilized microtubules (0−2 μM tubulin, 40 μM taxol) in a 220 μL reaction volume and allowed to incubate for 30 min. The reactions were subjected to centrifugation to separate free enzyme from that which sediments with the microtubules. An aliquot (110 μL) of the supernatant was removed and combined with 20 μL of 5× Laemmli sample buffer. The remaining supernatant was removed and discarded. ATPase buffer with 40 μM taxol was added to the tube without disturbing the pellet and removed to gently wash away any remaining supernatant. The pellet was resuspended in 55 μL of 5× Laemmli sample buffer plus 220 μL of ATPase buffer for SDS−PAGE. To determine the concentration of motor in the supernatant and pellet, the Coomassie Blue-stained gels were scanned and quantified using NIH Image Version 1.62. The ratio of the concentration of enzyme in the pellet to the concentration in the supernatant plus the pellet was plotted versus microtubule concentration and fit to the quadratic equation:

$$\text{Mt·}E/E_0 = 0.5\{(E_0 + K_d + \text{Mt}_0) - [(E_0 + K_d + \text{Mt}_0)^2 - (4E_0\text{Mt}_0)]^{1/2}\} \quad (5)$$

where Mt·E/E_0 is the fraction of E164A sedimenting with microtubules, E_0 is total E164A, Mt_0 is the total tubulin concentration, and K_d is the dissociation constant.

Molecular Modeling. The molecular modeling (Figure 1) was performed on a Silicon Graphics workstation using UCSF MidasPlus molecular interactive display and simulation software (Computer Graphics Laboratory, University of California, San Francisco, CA).

Molecular Docking. The atomic coordinates of the rat kinesin head domain from Sack et al. (*17*) and of α,β-tubulin (*50*) were computationally docked into the cryo-EM 3D reconstruction of microtubules decorated with monomeric rat kinesin head domains (*35*) using the software package O (*51*). Figure 13 was composed using Bobscript (*52*).

RESULTS

Glu^{164} (rat Glu^{158}) is located at the junction of β-strand 5a and loop 8b in a highly charged electrostatic environment (Figure 1). This glutamate could potentially interact with Arg^{286} (rat Arg^{280}) and Arg^{292} (rat Arg^{286}) on α-helix 5, which has been implicated in microtubule binding (*34*, *53*). Both loop L12 and α-helix 5 have been implicated in microtubule binding (*34*, *53*). In addition, the electrostatic region of rat Glu^{158} probably interacts with the opposing electrostatic face including residues Glu^{219}, Thr^{220}, and Glu^{221} of the partner head and Glu^{340} on α-helix 7 (all rat numbering). Kinesin motility along the microtubule requires that the stabilizing electrostatic interactions presented in Figure 1B, where kinesin is detached from the microtubule, be disrupted with rearrangement of electrostatic interactions occurring throughout the ATPase cycle. The experiments presented here analyze the ATPase pathway of Mt·E164A to understand the cooperative interactions between the motor domains and the structural transitions required for wild-type kinesin motility.

Steady-State ATPase Activity of E164A. The steady-state microtubule-activated ATPase kinetics reveal that the mutant motor exhibits a dramatic reduction in ATP turnover in comparison to wild-type kinesin: E164A $k_{cat} = 4.8\ s^{-1}$ versus $20-25\ s^{-1}$ for K401-wt (Figure 2 and Table 1). Furthermore, the results indicate that E164A binds both MgATP ($K_{m,ATP} = 21$ μM versus 61−96 μM for K401-wt) and microtubules ($K_{0.5,Mt} = 0.4$ μM versus 0.8−0.9 μM K401-wt) more tightly than observed for K401-wt. We cannot attribute the apparent aberrant behavior of E164A to a significant population of inactive motors. Figure 3 shows that >95% of the motor domains can bind and hydrolyze ATP in the absence of microtubules, keeping ADP tightly bound at the nucleotide binding site.

MantATP Binding. We began the pre-steady-state kinetic analysis of this dimeric mutant by examining ATP binding using the fluorescent analogue mantATP (Figure 4). A preformed Mt·E164A complex was rapidly mixed in the stopped-flow instrument with varying concentrations of mantATP, and the change in fluorescence was monitored. The exponential rate of the fluorescence enhancement increased linearly as a function of mantATP concentration. These data provided the second-order rate constant for

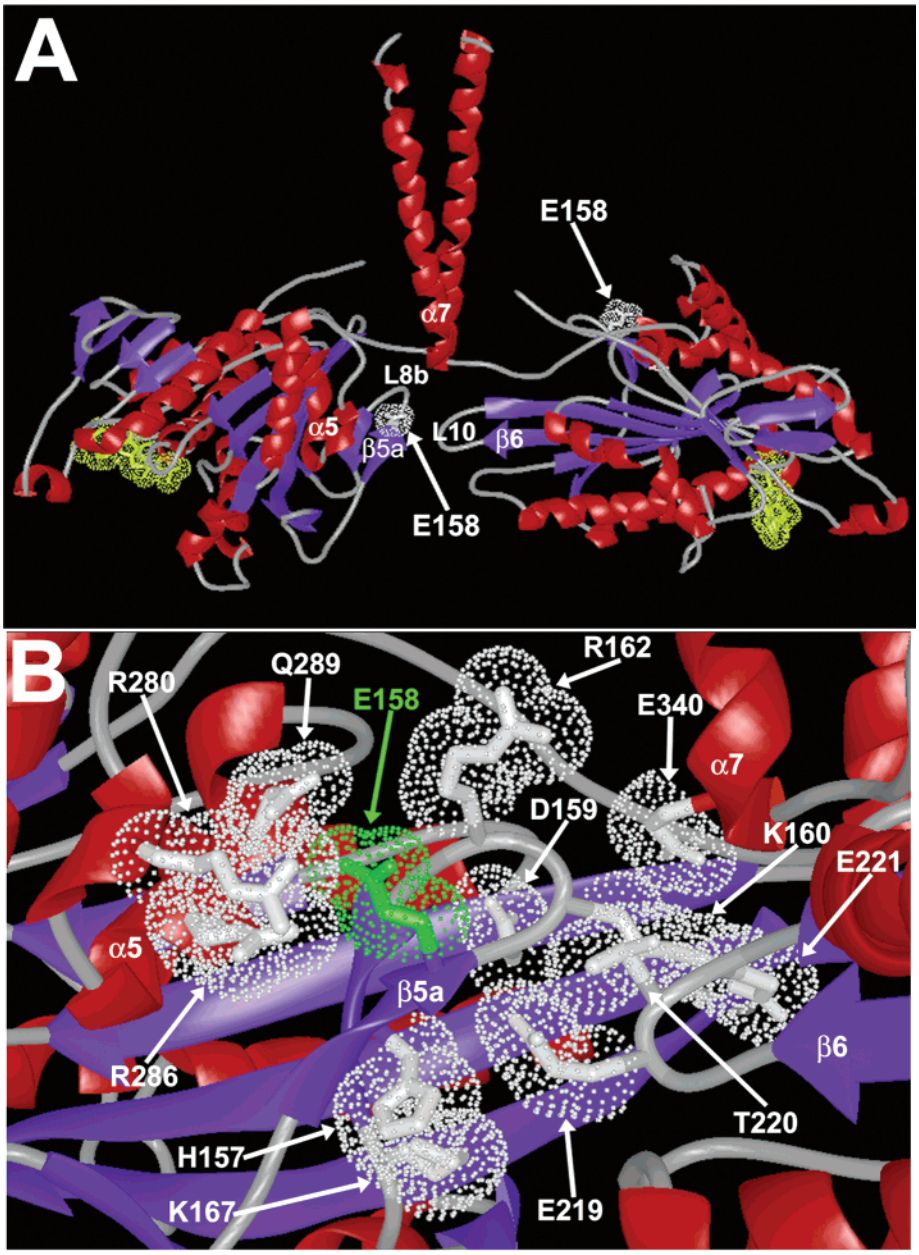

FIGURE 1: Location of the E164A mutation. Kinesin dimer model rat 3KIN (*16*). (A) Kinesin amino acid residues are designated by the rat sequence (rat E158, *Drosophila* E164, human E157). The active site of each motor domain is highlighted by the bound ADP (yellow), and the side chain of Glu[164] (rat E158) is identified in white, showing its location at the β-5a/loop 8b junction. (B) Detailed view of the *Drosophila* Glu[164] (rat E158) region. Glu[158], shown in green, lies in a highly charged electrostatic environment including Arg[280], Gln[289], Arg[286], Arg[162], His[157], Lys[167], Lys[160], and Asp[159] (all rat numbering). Furthermore, the electrostatic region of rat Glu[158] probably interacts with the opposing electrostatic face of the partner head including residues Glu[219], Thr[220], Glu[221], and Glu[340] on α7 (all rat numbering).

mantATP binding at $k_{+1} = 2.2\ \mu M^{-1}\ s^{-1}$, which was similar to that observed for K401-wt (Scheme 1 and Table 1).

Pre-Steady-State Kinetics of ATP Hydrolysis. Acid quench experiments were performed to determine the rate constant of ATP hydrolysis (Figure 5). A preformed Mt·E164A complex was rapidly mixed with varying concentrations of [α-^{32}P]MgATP. The reaction was quenched with formic acid, which terminated the reaction and released nucleotide that was bound at the active site. The transients presented in Figure 5A show the characteristic pre-steady-state burst of ADP·P_i product formation at the active site during the first ATP turnover, followed by a slower linear rate of product formation that corresponds to steady-state turnover. The exponential burst at the active site indicates that a step after ATP hydrolysis is rate-limiting. Furthermore, the results show that, at high ATP concentrations, ATP binding becomes faster than ATP hydrolysis. Because substrate binding is no longer limiting, the maximum rate constant for the exponential burst phase is the rate constant for ATP hydrolysis. This rate constant at 368 s^{-1} was significantly faster than ATP hydrolysis for K401-wt at ~100 s^{-1}. Furthermore, the $K_{d,ATP}$ at 16.5 μM obtained from Figure 5B provided direct evidence that the active site of the mutant was altered in its interactions with MgATP. The $K_{d,ATP}$ for K401-wt obtained from acid quench experiments was ~100 μM (*47*); therefore, these results indicate that E164A binds ATP with a tighter affinity than K401-wt.

The pre-steady-state burst amplitude, which represents the formation of the Mt·K·ADP·P_i intermediate, also increased as a function of ATP concentration (Figure 5C). However,

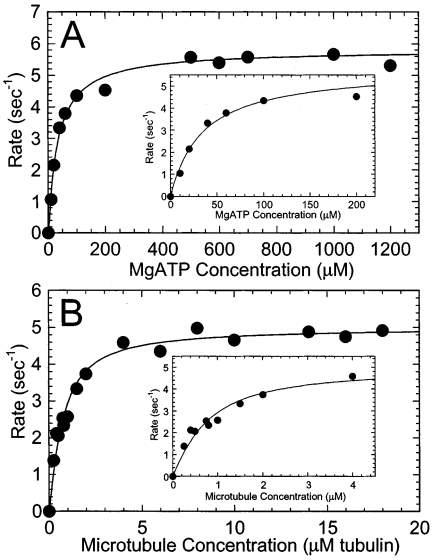

FIGURE 2: Steady-state ATPase activity of E164A. (A) The Mt·E164A complex was preformed with 0.5 μM motor and taxol-stabilized microtubules (16 μM tubulin) followed by incubation with [α-^{32}P]ATP (10−1200 μM). The fit of the data to a hyperbola provides $k_{cat} = 5.8 \pm 0.1$ s^{-1} and $K_{m,ATP} = 34.5 \pm 3.2$ μM. The inset shows the data for the lower ATP concentrations (average of nine experiments with nine E164A preparations): $k_{cat} = 4.9 \pm 0.5$ s^{-1} (range: 3.4−7.7 s^{-1}), $K_{m,ATP}$ 21.1 ± 2.6 μM (range: 10.1−34.5 μM). (B) The Mt·E164A complex (0.5 μM motor; microtubules at 0.25−20 μM tubulin) was incubated with 2 mM MgATP. The data were fit to eq 1, and $k_{cat} = 5.0 \pm 0.1$ s^{-1} and $K_{0.5,Mt} = 0.5 \pm 0.06$ μM. The inset shows data for the lower microtubule concentrations (average of three experiments with three E164A preparations): $k_{cat} = 4.4 \pm 0.86$ s^{-1} (range: 2.7−5.6 s^{-1}), $K_{0.5,Mt} = 0.42 \pm 0.09$ μM (range: 0.24−0.53 μM). Motor concentrations (E164A and K401-wt) are expressed throughout the manuscript as the concentration of ATP binding sites.

the maximum burst amplitude at 0.65 μM was significantly less than the 5 μM E164A sites used in the experiment. This result was unexpected because one assumes that at high ATP concentration, especially with tight ATP binding, each active site can bind and hydrolyze ATP. We anticipated that the burst amplitude would approach 5 μM because the enzyme concentration used in the experiment was 5 μM, and the active site titration of this protein preparation showed 4.8 μM active sites.

Pulse−chase experiments were conducted (Figures 6 and 7) to explore mechanistic reasons to account for the burst amplitude results. In these experiments, E164A was mixed with [α-^{32}P]MgATP for varying times after which excess nonradiolabeled MgATP was added as a chase. During the 0.9 s chase, [α-^{32}P]MgATP tightly bound at the active site will partition toward ATP hydrolysis, yet [α-^{32}P]MgATP more weakly bound will dissociate from the active site and become diluted by the nonradiolabeled ATP chase.

A preformed Mt·E164A complex was rapidly mixed with [α-^{32}P]MgATP followed by either an acid quench or a 5 mM MgATP chase for direct comparison of time courses at 25 μM, 50 μM, and 100 μM [α-^{32}P]MgATP (Figure 6). The results (exponential burst phase) show that ATP binding is faster than ATP hydrolysis. Furthermore, ATP binding is sufficiently tight to permit accumulation of a stable Mt·K·ATP intermediate prior to ATP hydrolysis. The pathway for E164A is dramatically different from K401-wt, where the acid quench and pulse−chase transients were quite similar because of the fast ATP off rate (k_{-1}) relative to ATP hydrolysis (k_{+2}) (see Figure 1 of ref *47*). These results suggest that the ATPase mechanism for E164A is altered, and there is not a significant ATP off rate as observed for K401-wt.

Pulse−Chase Kinetics of ATP Binding. To explore the reduced burst amplitude observed in the acid quench experiments, pulse−chase experiments were performed as a function of [α-^{32}P]MgATP concentration. The results presented in Figure 6 indicated that ATP bound tightly to the active site to form a stable Mt·K*·ATP intermediate. The nonradioactive MgATP chase drives the reaction toward the Mt·K·ADP·P_i intermediate; therefore, at high [α-^{32}P]MgATP all active sites should be saturated with radiolabeled ATP and detected after the pulse−chase as [α-^{32}P]ADP. The burst amplitude data presented in Figure 7C show an ATP-dependent increase in the burst amplitude; however, the maximum burst amplitude at 1.7 μM of 5 μM sites indicates that only 34% of the sites were catalytic. These pulse−chase data (Figure 7B) also show saturation of the exponential burst at 521 s^{-1} ($k_{+1'}$). This rate constant is attributed to a rate-limiting conformational change to form the Mt·K*·ATP intermediate that proceeds directly to ATP hydrolysis (Scheme 1). Two-step ATP binding was also observed for K401-wt, where the exponential burst rate saturated at 239 s^{-1} (*10*, *47*; Table 1).

ATP-Promoted Dissociation of the Mt·E164A Complex. To examine the effect of the E164A mutation on motor domain detachment from the microtubule, changes in turbidity were monitored in the stopped-flow instrument. The preformed Mt·E164A complex was rapidly mixed with 1 mM MgATP plus 100 mM KCl. This experimental design was required to measure the dissociation kinetics of K401-wt because of kinesin's high processivity (*7*, *10*). The rationale is that ATP promotes motor detachment from the microtubule, and the salt weakens the affinity of the motor as it attempts to rebind the microtubule. Therefore, a change in turbidity can be detected. The results in Figure 8 show that dissociation of the Mt·K401-wt complex occurred at 12 s^{-1} as reported previously (*7*, *10*). Although the rate constant for dissociation of the Mt·E164A complex was measured at 5.1 s^{-1}, the amplitude associated with the signal was quite small relative to the amplitude of the K401-wt transient. The experiment was repeated at 1 mM MgATP with increasing concentrations of KCl, yet salt concentrations as high as 500 and 800 mM KCl did not drive the E164A dissociation transients to amplitudes of the K401-wt transient. Note that the optical signal for the control, microtubules + ATP + 800 mM KCl, did not change, suggesting that the turbidity signal associated with the E164A transients did not represent microtubule depolymerization. These data indicate that ATP does not readily promote detachment of the mutant motor from the microtubule.

Microtubule Association. Because of the unusual dissociation kinetics observed with the mutant, we pursued experiments to determine whether Mt·E164A complex formation was aberrant. Equilibrium binding experiments were performed (Figure 8B), and the data show that all E164A motors partitioned with the microtubules during centrifugation. These results demonstrate that E164A can bind microtubules; therefore, the aberrant dissociation kinetics cannot be attributed to only a few motors bound to microtubules at the

Table 1: Microtubule−Kinesin Constants

		experimentally determined		computer simulation[f]
	rate constants	E164A	K401-wt	K401-wt
k_{+1}	mantATP binding[a]	$2.2 \pm 0.1\ \mu M^{-1}\ s^{-1}$ $k_{off} = 20.6 \pm 3.4\ s^{-1}$	$1.1\ \mu M^{-1}\ s^{-1}$ [a] $k_{off} = 9.8\ s^{-1}$	$2\ \mu M^{-1}\ s^{-1}$ $k_{off} = 120\ s^{-1}$
k_{+2}	acid quench[b]	$368 \pm 20.4\ s^{-1}$ $K_{d,ATP} = 16.5 \pm 5\ \mu M$ Amp[g] = 0.13/site	$93\ s^{-1}$ [b] $K_{d,ATP} = 87\ \mu M$ Amp = 0.55/site	$100\ s^{-1}$
$k_{+1'} + k_{-1'}$	pulse−chase[b]	$521 \pm 43.1\ s^{-1}$ $K_{d,ATP} = 44.2 \pm 12.6\ \mu M$ Amp = 0.34/site	$239\ s^{-1}$ [b] $K_{d,ATP} = 70\ \mu M$ Amp = 0.73/site	
k_{+3}	ATP-promoted microtubule dissociation[c]	does not dissociate	$12-14\ s^{-1}$ [c]	$50\ s^{-1}$
k_{+4}	P_i release[d]		$13\ s^{-1}$ [d]	$>150\ s^{-1}$
k_{+5}	microtubule association[c]	$9.2 \pm 0.6\ \mu M^{-1}\ s^{-1}$	$10-20\ \mu M^{-1}\ s^{-1}$ [c]	$11\ \mu M^{-1}\ s^{-1}$
k_{+6}	mantADP release, both heads[e]	$71.6 \pm 3.2\ s^{-1}$ $K_{0.5,Mt} = 4.1 \pm 0.7\ \mu M$	$>200\ s^{-1}$ [e] $K_{0.5,Mt} = 15\ \mu M$	$300\ s^{-1}$
	MantADP release, head 2[e]	ATP $48.0 \pm 1.3\ s^{-1}$ ADP $35.0 \pm 0.8\ s^{-1}$	ATP $>100\ s^{-1}$ [e] ADP $6.6\ s^{-1}$ [e]	$200\ s^{-1}$
k_{cat}		$4.9 \pm 0.5\ s^{-1}$	$20-25\ s^{-1}$	
$K_{m,ATP}$		$21.1 \pm 2.6\ \mu M$	$61-96\ \mu M$	
$K_{0.5,Mt}$		$0.42 \pm 0.09\ \mu M$	$0.8-0.9\ \mu M$	

[a] MantATP binding (*11*). [b] Rapid quench (*47*). [c] Turbidity (*7*, *11*). [d] MDCC−PBP (*7*, *11*). [e] MantADP competed with excess unlabeled MgATP or MgADP (*6*, *7*, *11*, *48*). [f] Computer simulations (*11*). [g] Amp, burst amplitude.

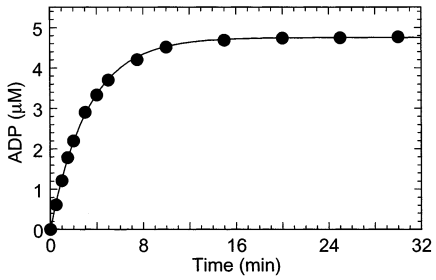

FIGURE 3: Active site titration. E164A·ADP at 5 μM was incubated with trace amounts of [α-^{32}P]ATP in the absence of microtubules, and the radiolabeled ADP produced was plotted as a function of time. The fit of the data to a single-exponential function provided an amplitude of $4.75 \pm 0.01\ \mu M$, which represents the E164A motor domains that were competent to bind and hydrolyze [α-^{32}P]ATP.

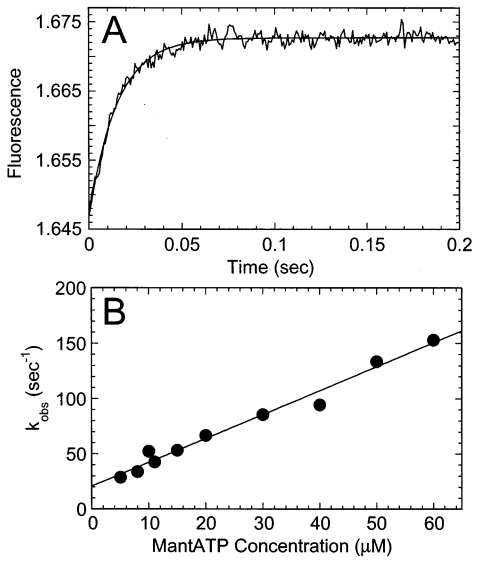

FIGURE 4: Pre-steady-state kinetics of mantATP binding. A preformed Mt·E164A complex (3 μM E164A, 12 μM tubulin) was rapidly mixed in the stopped-flow instrument with varying concentrations of mantATP (5−60 μM). (A) A representative transient at 20 μM mantATP where the smooth line is the fit of the data to a single-exponential function: $k_{obs} = 66.9 \pm 1.8\ s^{-1}$. (B) The exponential rate of the observed process increased linearly as a function of mantATP concentration. The data were fit to eq 2, which provided the second-order rate constant for mantATP binding: $k_{+1} = 2.2 \pm 0.1\ \mu M^{-1}\ s^{-1}$ and $k_{off} = 20.6 \pm 3.4\ s^{-1}$.

start of the dissociation experiment. The data also indicate that at 1 μM tubulin ~90% of mutant motors (2 μM E164A) partition with microtubules, suggesting a stoichiometry of 2 heads per tubulin heterodimer rather than the 1:1 stoichiometry reported previously for K401-wt (*54*).

We also evaluated Mt·E164A complex formation by measuring the association kinetics in the stopped-flow instrument (Figure 9). In this experiment, E164A·ADP was rapidly mixed with varying concentrations of microtubules. The exponential phase of the association kinetics increased as a function of microtubule concentration, and the fit of the data to a linear function provided the second-order rate constant for microtubule association, $k_{+5} = 9.2\ \mu M^{-1}\ s^{-1}$ (Scheme 1). This rate constant is similar to the constant measured for K401-wt at 11 $\mu M^{-1}\ s^{-1}$ (Table 1) (*7*, *12*), and the *y*-intercept at zero reinforces the interpretation that E164A binds microtubules tightly to form the Mt·E164A complex.

MantADP Release from Both Heads. The kinetics of ADP release from the Mt·E164A·ADP intermediate were determined using the fluorescent analogue of ADP, mantADP (Figure 10). The E164A·mantADP complex was preformed such that E164A contained mantADP bound to both heads. The complex was rapidly mixed in the stopped-flow instrument with varying concentrations of microtubules plus 1 mM MgATP. The MgATP present in the reaction acts to block any rebinding of the mantADP to the active site. MantADP release was activated by microtubules with the maximum rate constant at 72 s^{-1} with $K_{0.5,Mt} = 4.1\ \mu M$. MantADP release from E164A is slower than K401-wt ($k_{max} = 200-300\ s^{-1}$). Furthermore, the $K_{0.5,Mt}$ at 4.1 μM is significantly tighter than that observed for K401-wt at 15 μM (*7*). These data also reflect the higher affinity of E164A for microtubules.

MantADP Release from Head 2 Initiated by ATP. To evaluate the possibility of a loss of motor domain cooper-

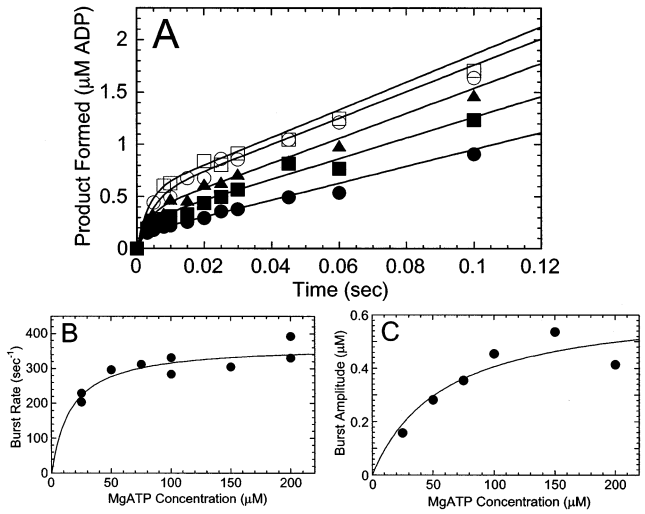

FIGURE 5: Pre-steady-state kinetics of ATP hydrolysis. A preformed Mt·E164A complex (5 μM E164A, 15 μM tubulin) was rapidly mixed with varying concentrations of [α-^{32}P]MgATP in a chemical quench-flow instrument. The reaction times varied from 3 to 400 ms, and the data were fit to eq 4. (A) Transients for ATP hydrolysis in the presence of 25 μM (●), 50 μM (■), 75 μM (▲), 100 μM (○), and 150 μM (□) [α-^{32}P]MgATP. Only the first 120 ms of each transient is shown to expand the time domain of the initial burst phase. (B) The rate constants of the pre-steady-state burst phase (k_b) determined from transients in panel A as well as other experiments not shown were plotted as a function of [α-^{32}P]MgATP concentration. The fit of the data to a hyperbola provided the maximum rate constant for the exponential burst at 368 ± 20.4 s^{-1} and $K_{d,ATP}$ = 16.5 ± 5 μM. (C) The amplitudes of the pre-steady-state burst phase determined for each of the transients in panel A as well as other experiments not shown were plotted as a function of [α-^{32}P]MgATP concentration. The data were fit to a hyperbola which provided the maximum burst amplitude = 0.65 ± 0.13 μM (0.13/site) and $K_{d,ATP}$ = 59.1 ± 32.4 μM.

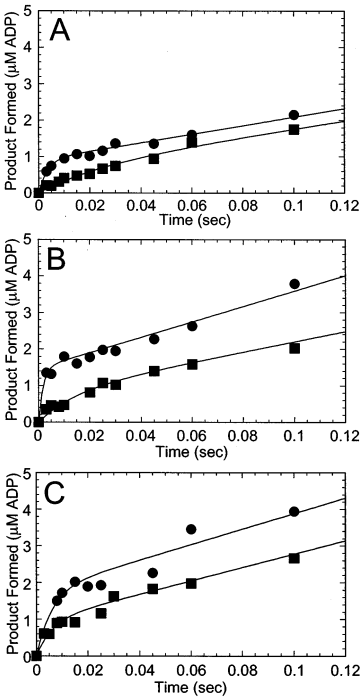

FIGURE 6: Pre-steady-state kinetics of ATP binding and hydrolysis. A preformed Mt·E164A complex (5 μM E164A, 15 μM tubulin) was rapidly mixed with [α-^{32}P]MgATP and reacted for 3−400 ms. The time courses of ATP binding (pulse−chase, ●) and ATP hydrolysis (acid quench, ■) were determined for three different [α-^{32}P]MgATP concentrations (A, 25 μM; B, 50 μM; C, 100 μM). The smooth lines are the fit of the data to eq 4, which provided the burst amplitude (A) and burst rate (k_b) for both rapid quench conditions.

ativity, a series of mantADP dissociation experiments were performed (Figures 11 and 12). It has been shown for wild-type kinesin that ADP release is fast from the first head upon collision with the microtubule, but ADP release from the second head is delayed until the first head can bind ATP (*6*, *8*, *9*). In the experiment presented in Figure 11, the Mt·E164A·mantADP complex (5 μM E164A, 2.5 μM mantADP, 15 μM tubulin) was preformed such that mantADP was at half the concentration of active sites. One head of the dimer will be tightly bound to the microtubule and free of nucleotide. The second head will be detached or weakly bound to the microtubule, and mantADP partitions to this detached head. Therefore, mantADP release from the high-affinity site will be measured by this experimental design (*9*). The Mt·E164A·mantADP complex was rapidly mixed in the stopped-flow instrument with varying concentrations of MgATP. It is assumed that ATP binds to the head that is free of nucleotide and bound to the microtubule, causing it to elicit a signal to the second head to bind to the microtubule and release its mantADP. The maximum rate constant of mantADP release from the high-affinity site initiated by ATP was 48 s^{-1}. This rate of mantADP release from head 2 promoted by ATP was significantly slower than observed for wild-type kinesin at >100 s^{-1} (*6*, *9*).

MantADP Release from Head 2 Initiated by ADP. To evaluate the motor domain cooperativity, the experiment was repeated, but ADP was used to elicit the signal to the second head for mantADP release (Figure 12). The preformed Mt·E614A·mantADP complex was rapidly mixed with varying concentrations of MgADP. The maximum rate constant for mantADP release from the second head of E164A initiated by ADP was 35 s^{-1}. This rate constant for E164A was significantly faster than the rate constant determined for K401-wt at 5−6 s^{-1} (*6*, *9*). These mantADP results (Figures 11 and 12) suggest that head 1 cannot distinguish ATP from ADP and/or head 1 cannot communicate its nucleotide state to head 2. The intermolecular motor domain cooperativity in the dimer is clearly disrupted by the alanine substitution at Glu^{164}.

Microtubule−Kinesin Interface. The mechanistic results indicate that the mutant motor exhibits much higher affinity

Scheme 1

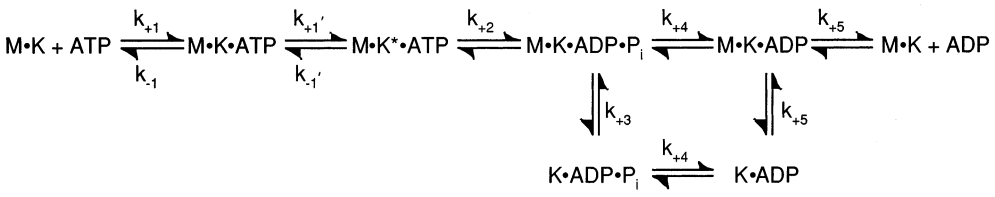

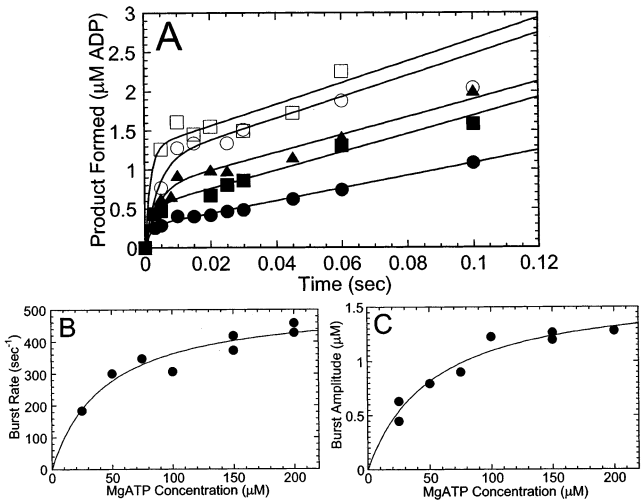

FIGURE 7: Pulse−chase kinetics of ATP binding. A preformed Mt·E164A complex (5 μM E164A, 15 μM tubulin) was rapidly mixed with varying concentrations of [α-^{32}P]MgATP. The reaction times varied from 3 to 400 ms, followed by a 5 mM MgATP chase for 0.9 s and subsequent acid quench. The data were fit to eq 4 to obtain the amplitude and exponential rate constant of the pre-steady-state burst phase. (A) Transients for ATP binding in the presence of 25 μM (●), 50 μM (■), 100 μM (▲), 150 μM (○), and 200 μM (□) [α-^{32}P]MgATP. (B) The rate constants of the pre-steady-state burst phase determined from transients in panel A as well as other experiments not shown were plotted as a function of [α-^{32}P]MgATP concentration. The fit of the data to a hyperbola provides the maximum rate constant for the burst phase, $k_b = 521 \pm 43.1$ s^{-1} and $K_{d,ATP} = 44.2 \pm 12.6$ μM. (C) The amplitudes of the pre-steady-state burst phase determined from the transients in panel A as well as other experiments not shown were plotted as a function of [α-^{32}P]MgATP concentration. The data were fit to a hyperbola with 1.7 ± 0.14 μM (0.34/site) as the maximum burst amplitude and $K_{d,ATP} = 52.3 \pm 12.2$ μM.

for both ATP and the microtubule. Second, E164A does not appear to detach from the microtubule in the dissociation kinetic experiment. To interpret the mechanistic data in the context of microtubule−kinesin structural models, Glu^{164} (rat Glu^{158}) was identified in the model docking rat kinesin and tubulin crystal structures in the scaffold of a microtubule−kinesin complex (Figure 13). Rat Glu^{158} is located at the β-strand 5a/loop 8b junction and projects toward the center of the microtubule binding surface. Although the proximity of Glu^{164} (rat Glu^{158}) at the microtubule−motor interface is intriguing, the dissociation kinetics at high salt concentrations rule out interpretations that argue for a more stable Mt·E164A intermediate because of additional favorable electrostatic interactions formed with microtubule amino acids by the glutamate to alanine substitution. However, if additional hydrophobic interactions were formed between kinesin and the microtubule, the salt in the dissociation experiment would stabilize this contact interface.

DISCUSSION

Drosophila kinesin Glu^{164} was identified through a genetic screen to be an amino acid essential for kinesin function in vivo (*44*), and our analysis of the mutant dimeric kinesin, E164A, has revealed an unusual mechanistic phenotype. The kinetic and thermodynamic constants are summarized in Table 1, and the results are discussed in the context of the model for kinesin stepping presented in Figure 14.

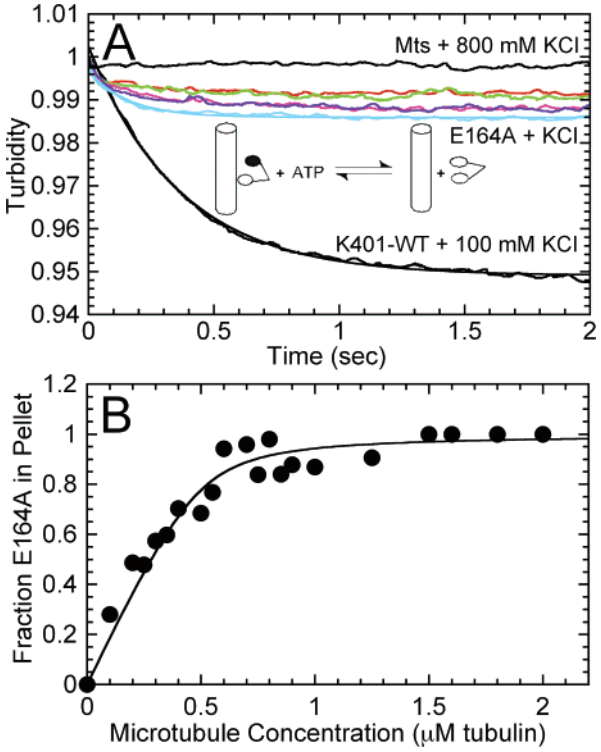

FIGURE 8: Evaluation of Mt·E164A complex stability. (A) The preformed Mt·E164A complex (3 μM E164A, 2.9 μM tubulin) was rapidly mixed with 1 mM MgATP plus KCl: 100 mM (orange), 200 mM (green), 300 mM (pink), 400 mM (dark blue), and 800 mM (aqua). For the trace representing E164A with 100 mM KCl (orange), the smooth line is the fit of the data to a single-exponential function and provides the rate of the initial exponential phase at $k_{obs} = 5.1 \pm 0.3$ s^{-1}. For comparison, the kinetics of K401-wt (3 μM E164A, 2.9 μM tubulin) are shown at 1 mM MgATP + 100 mM KCl ($k_{obs} = 11.5 \pm 0.5$ s^{-1}). The data were fit to two exponential functions for K401-wt. (B) Mt·E164A complexes were formed at various concentrations of microtubules in the absence of nucleotides (2 μM E164A, 0−2 μM microtubules, 40 μM taxol) and allowed to reach equilibrium, followed by centrifugation. The fraction of E164A in the pellet was graphed as a function of microtubule concentration and fit to eq 5: $K_{d,M_t} = 0.032 \pm 0.016$ μM. The average of four experiments is 0.062 ± 0.027 μM (range: 0.016−0.13 μM). Note that all E164A partitioned with microtubules.

Mechanistic Consequences of Glutamate to Alanine Substitution. The results presented clearly indicate that the behavior of E164A is aberrant. The steady-state results show a dramatic reduction in the k_{cat} as well as a significantly higher affinity of E164A for both microtubules and ATP (Figure 2). The rapid quench data (Figure 5) provide evidence that ATP hydrolysis (368 s^{-1}) is significantly faster and ATP binding tighter ($K_{d,ATP} = 16.5$ μM). In fact, the results indicate that ATP hydrolysis on head 1 occurs prior to ADP release from head 2 (Figure 14) because mantADP release is slowed to 72 s^{-1} when E164A collides with the microtubule.

The experiments that explored communication between the motor domains (Figures 11 and 12) indicate that signaling is aberrant. For kinesin, ATP binding at head 1 (Figure 14, species 2) leads to the plus-end directed motion of the neck linker to position head 2 at the next microtubule binding site (*31*), followed by rapid ADP release (*6*, *8*, *9*). For E164A, mantADP release from head 2 initiated by ATP was 48 s^{-1}, which was significantly slower than observed for K401-wt

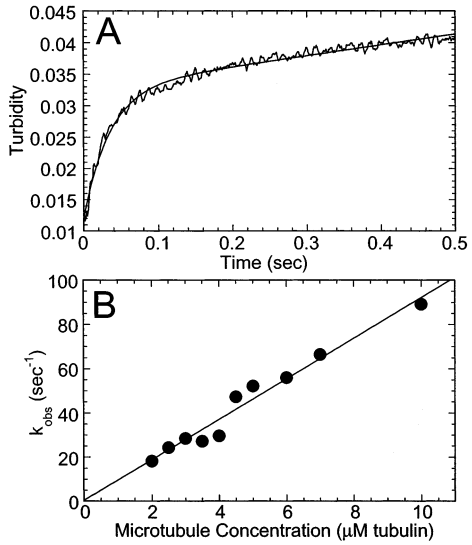

FIGURE 9: E164A−microtubule association kinetics. E164A·ADP at 2.5 μM was rapidly mixed with varying concentrations of microtubules (2−10 μM). (A) A representative stopped-flow transient at 3 μM microtubules is shown where the smooth line is the fit of the data to two exponential functions. The observed rate constant of the initial exponential phase was 28.5 ± 0.6 s^{-1}. (B) The rate constant from the initial exponential phase increased as a function of microtubule concentration. The data were fit to eq 3, which provided the second-order rate constant for microtubule association, k_{+5} = 9.2 ± 0.6 μM^{-1} s^{-1}.

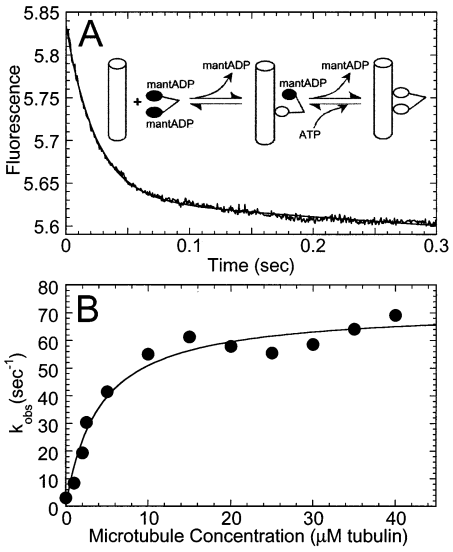

FIGURE 10: Kinetics of mantADP release from both heads. The E164A·mantADP complex (3 μM E164A, 6 μM mantADP) was preformed such that E164A contained mantADP bound to both heads. The complex was rapidly mixed in the stopped-flow instrument with varying concentrations of microtubules (1−40 μM tubulin) plus 1 mM MgATP. (A) A representative transient is shown at 5 μM microtubules. The smooth line represents the fit of the data to two exponential functions: (1) 49.8 ± 1.1 s^{-1}, relative amplitude 0.175, and (2) 8.7 ± 0.7 s^{-1}, relative amplitude 0.06. (B) The rate constant from the initial exponential phase increased as a function of microtubule concentration. The fit of the data to a hyperbola provided the maximum rate constant of mantADP release: k_{max} = 71.6 ± 3.2 s^{-1} with $K_{0.5,Mt}$ at 4.1 ± 0.7 μM.

at >100 s^{-1}. However, mantADP release from head 2 initiated by MgADP was quite fast at 35 s^{-1} and similar to the rate observed with ATP. For wild-type kinesin, mantADP release initiated by ADP occurred at 5−6 s^{-1} (*6*, *9*).

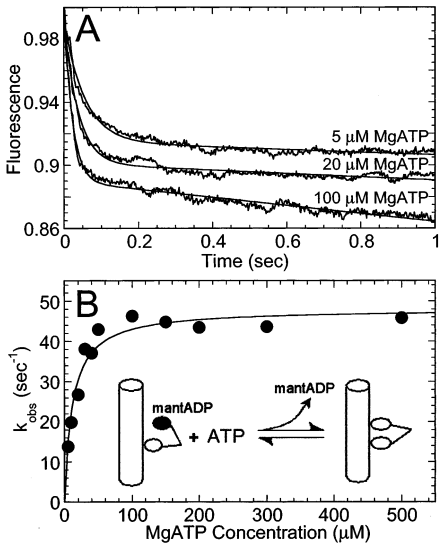

FIGURE 11: MantADP release from head 2 initiated by ATP. The Mt·E614A·mantADP complex (5 μM E164A, 2.5 μM mantADP, 15 μM tubulin) was rapidly mixed with increasing concentrations of MgATP (5−1000 μM). (A) Transients are shown for 5 μM, 20 μM, and 100 μM MgATP. (B) The observed exponential rate constants of the MgATP-dependent fluorescence change were plotted as a function of MgATP concentration. The data were fit to a hyperbola, providing the maximum rate constant of mantADP release from the second head, k_{obs} = 48.0 ± 1.3 s^{-1}.

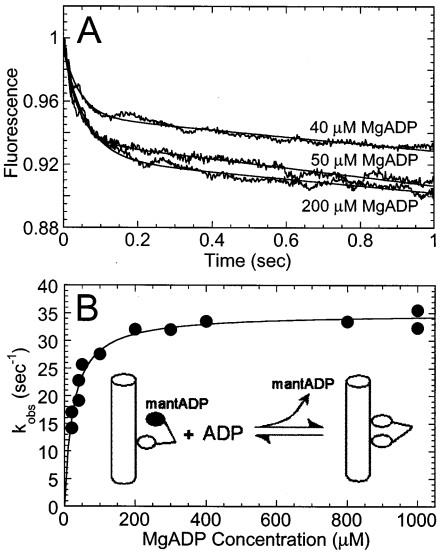

FIGURE 12: MantADP release from head 2 initiated by ADP. The preformed Mt·E614A·mantADP complex (5 μM E164A, 2.5 μM mantADP, 15 μM tubulin) was rapidly mixed with increasing concentrations of MgADP (20−1000 μM). (A) Transients are shown for 40 μM, 50 μM, and 200 μM MgADP. (B) The rate constants of the MgADP-dependent fluorescence change were plotted as a function of MgADP concentration. The data were fit to a hyperbola which yielded the maximum rate of mantADP release from the second head of E164A at 35.0 ± 0.8 s^{-1}.

These kinetic results indicate that the glutamate to alanine substitution has altered the switch I and switch II interactions with nucleotide and affected the path of communication from the active site to the microtubule. This miscommunication may involve a series of structural interactions via helix α5 to loop L12 to relay helix α4 (switch II) to switch I interactions with the nucleotide.

Another intriguing observation is provided by the pulse−chase rapid quench kinetics for the Mt·E164A complex

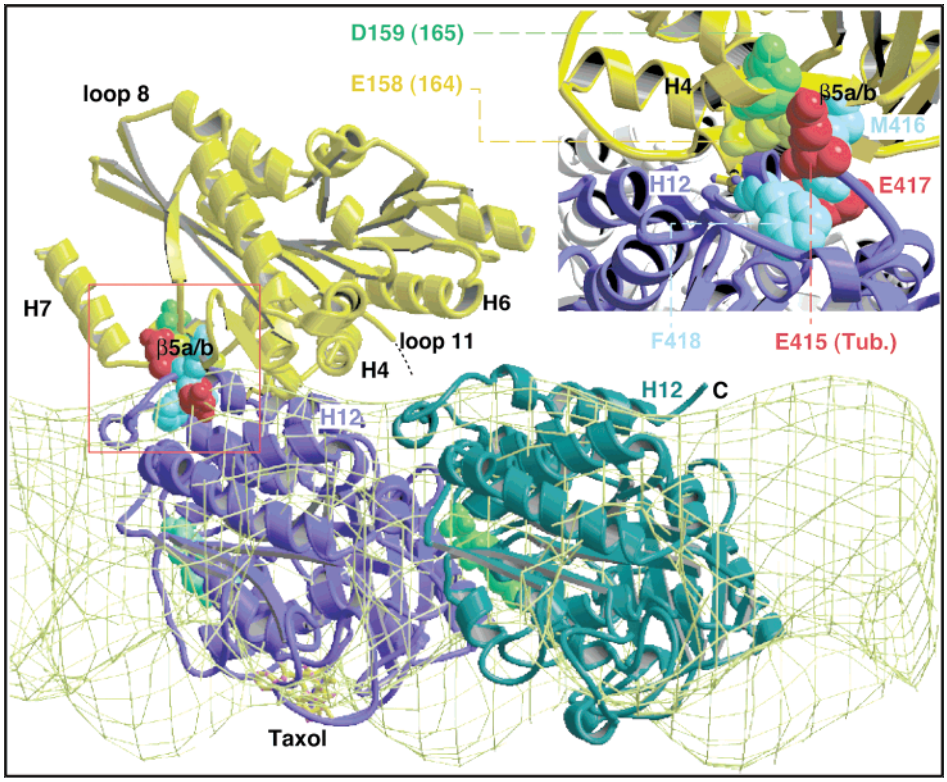

FIGURE 13: Model of the microtubule−kinesin interface. The potential interactions of *Drosophila* Glu[164] (rat E158) at the β-sheet 5a/loop 8b junction with microtubule amino acids were determined by docking monomeric kinesin [rat 2KIN (*17*)] into the 3D scaffold of a microtubule−kinesin complex. In this view, the plus end is to the left. The kinesin motor domain is shown in yellow, and amino acid residues are designated by the rat sequence (rat Glu[158], Asp[159]; *Drosophila* Glu[164], Asp[165]; human Glu[157], Asp[158]). The α-tubulin (teal) and β-tubulin (purple) dimer is shown with nucleotide bound (green) at the active sites and taxol (yellow) bound at β-tubulin. Kinesin and the microtubule interact predominantly through tubulin helices H11 and H12. Note that Glu[415], Met[416], Glu[417], and Phe[418] are β-tubulin residues, which are in close proximity to Glu[158]. The key structural elements for microtubule binding in kinesin are α4-L12-α5, L11, and β5a,b.

(Figures 6 and 7). The burst amplitude was 0.34/site, which is significantly less than the expected 1 per site. Also, the kinetics for mantATP binding (Figure 4) at each mantATP concentration fit to a single-exponential function. These kinetics were unexpected because K401-wt required a double-exponential function that was correlated with mant-ATP binding to each head of the dimer. These results suggest that head 2 may not bind ATP, and if head 2 were able to bind ATP, then ATP hydrolysis did not occur (species 7, Figure 14).

Model for Mt·E164A ATPase and Implications for Kinesin Mechanochemistry. In Figure 14, we present a model for kinesin motility based on mechanistic results (*6*, *8*, *9*, *11*, *13*, *39*, *40*, *43*, *47*, *55*) as well as those from Rice et al. (*31*) and Schnitzer et al. (*41*). The cycle begins as the first motor domain binds the microtubule with rapid ADP release. ATP binding at head 1 leads to the series of conformational changes to dock the neck linker of head 1 onto the motor core and to propel head 2 forward to the next binding site on the microtubule (species 4). Microtubule association activates ADP release from head 2, but ATP hydrolysis on head 1 is required for head 2 to bind tightly to the microtubule (species 5). In this model, head 2 must lock down onto the microtubule before head 1 can undergo dissociation. The strain generated in species 5 weakens the affinity of head 1, resulting in concomitant phosphate release and dissociation.

We propose for E164A that the more rapid ATP hydrolysis at head 1 results in head 2 becoming tightly bound to the microtubule prior to ADP release at head 2 (species 5). The conformation of E164A head 2 would alter the active site contacts with nucleotide such that ADP release is slowed dramatically. Furthermore, the pulse−chase rapid quench results suggest that E164A is stalled at species 5 and 6, and the structural transitions that permit ATP binding and ATP hydrolysis are prevented on head 2 (species 7). These results appear inconsistent with the inchworm model as originally proposed by Hua et al. (*56*). The inchworm model required that one head of the dimer be noncatalytic. For E164A in solution >95% of the sites are catalytic (Figure 3), yet the acid quench and pulse−chase kinetics indicate that, for the Mt·E164A complex, only one site is able to bind and hydrolyze ATP. The E164A dimer cannot proceed forward in its ATPase cycle because head 2 cannot bind and hydrolyze ATP. In contrast, all sites of K401-wt were competent to bind and hydrolyze ATP (*7*, *47*).

The rate-limiting step of the E164A ATPase pathway would appear to be detachment from the microtubule. One hypothesis that we are evaluating is whether head 1 detachment from the microtubule or phosphate release is the key step in controlling the conformational transitions that permit ATP binding and ATP hydrolysis to head 2 (species 5−7).

Structural Hypotheses for the E164A Mechanistic Phenotype. In the crystal structure of kinesin (Figure 1), the Glu[164] residue lies at the interface between the two motor domains and is in a highly charged electrostatic environment. However, this structure represents kinesin in solution and may not reflect the environment when kinesin is bound to

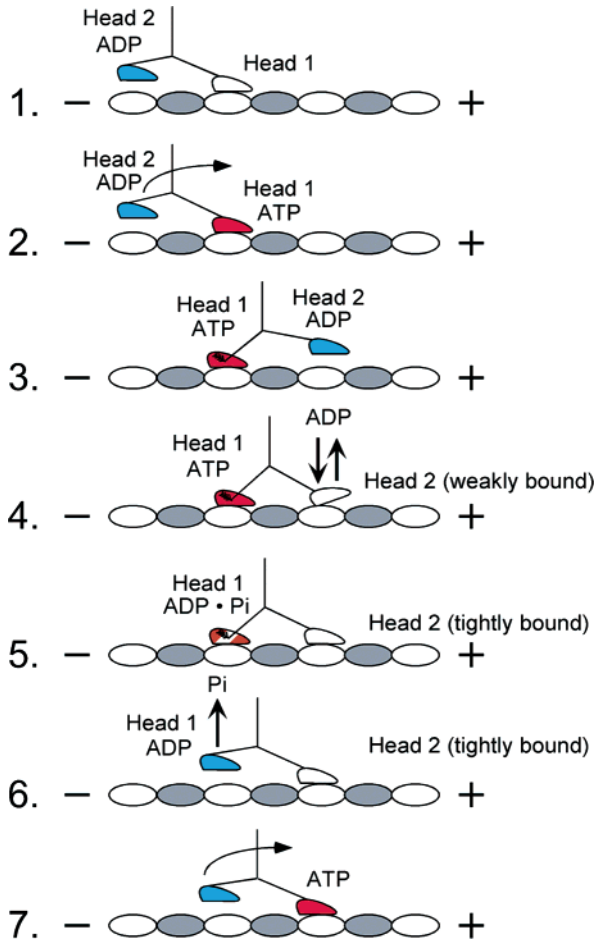

FIGURE 14: Model for kinesin stepping. The cycle begins as head 1 binds the microtubule with rapid ADP release. ATP binding at head 1 leads to the plus-end directed motion of the neck linker to position head 2 forward at the next microtubule binding site. ATP binding at head 1 is sufficient to promote head 2 association with the microtubule followed by rapid ADP release. ATP hydrolysis at head 1 locks head 2 onto the microtubule in a tight binding state. The strain induced by the tight binding of head 2 weakens the affinity of head 1 and results in its detachment from the microtubule concomitant with P_i release. The active site of head 2 is now accessible for ATP binding, and the cycle is repeated.

the microtubule. It appears more plausible that the mechanistic consequences result because of the loss of interactions with helix α5 normally mediated by negatively charged Glu[164]. For example, *Drosophila* Thr[291] (rat Thr[285]) is located on helix α5, and the genetic mutant T291M motor also showed aberrant interaction with nucleotide (*48*). In both cases, abnormal nucleotide behavior from the amino acid substitution may disrupt the local environment within one head and the structural accommodation transmitted back to the active site via a cascade effect from helix α5 to L12, α4, and the switch I−switch II interactions with nucleotide. In addition, Glu[164] projects toward the microtubule binding face and is in close proximity to key tubulin residues on tubulin helix α12 including Glu[415], Glu[417], Phe[418], and Met[416] (Figure 13). These results suggest that the alanine substitution may disrupt the normal repelling effect of Glu[164] with the tubulin α12 glutamates, Glu[415] and Glu[417]. Furthermore, additional hydrophobic interactions may be created by the alanine substitution. Note that Phe[418] as well as Met[416] on *β*-tubulin is also in close proximity; therefore, additional hydrophobic interactions may potentially stabilize the Mt·E164A complex, thus preventing dissociation. The dissociation kinetics as a function of salt concentration (Figure 8) favor this interpretation, although the observed behavior of E164A probably results because of aberrant interactions at helix α5 as well as stabilizing interactions at the microtubule interface. Our future studies are directed to explore the role of Glu[164] for kinesin mechanochemistry and to dissect the transitions from ATP hydrolysis on the rearward head that permit ATP binding and ATP hydrolysis on the forward motor domain.

ACKNOWLEDGMENT

We thank Brian Robertson for help with protein purification and technical assistance and Dr. Steven Rosenfeld (University of Alabama at Birmingham) for thoughtful reading of the manuscript during its preparation.

REFERENCES

1. Vale, R. D., and Milligan, R. A. (2000) *Science 288*, 88−95.
2. Schief, W. R., and Howard, J. (2001) *Curr. Opin. Cell Biol. 13*, 19−28.
3. Taylor, E. W., and Borisy, G. G. (2000) *J. Cell Biol. 151*, F27−F29.
4. Woehlke, G., and Schliwa, M. (2000) *Nat. Rev. Mol. Cell Biol. 1*, 50−58.
5. Sablin, E. P. (2000) *Curr. Opin. Cell Biol. 12*, 35−41.
6. Gilbert, S. P., Moyer, M. L., and Johnson, K. A. (1998) *Biochemistry 37*, 792−799.
7. Gilbert, S. P., Webb, M. R., Brune, M., and Johnson, K. A. (1995) *Nature 373*, 671−676.
8. Hackney, D. D. (1994) *Proc. Natl. Acad. Sci. U.S.A. 91*, 6865−6869.
9. Ma, Y. Z., and Taylor, E. W. (1997) *J. Biol. Chem. 272*, 724−730.
10. Ma, Y. Z., and Taylor, E. W. (1995) *Biochemistry 34*, 13242−13251.
11. Moyer, M. L., Gilbert, S. P., and Johnson, K. A. (1998) *Biochemistry 37*, 800−813.
12. Mandelkow, E., and Johnson, K. A. (1998) *Trends Biochem. Sci. 23*, 429−433.
13. Rosenfeld, S. S., Xing, J., Jefferson, G. M., Cheung, H. C., and King, P. H. (2002) *J. Biol. Chem. 277*, 36731−36739.
14. Song, Y. H., Marx, A., Muller, J., Woehlke, G., Schliwa, M., Krebs, A., Hoenger, A., and Mandelkow, E. (2001) *EMBO J. 20*, 6213−6225.
15. Kikkawa, M., Sablin, E. P., Okada, Y., Yajima, H., Fletterick, R. J., and Hirokawa, N. (2001) *Nature 411*, 439−445.
16. Kozielski, F., Sack, S., Marx, A., Thormahlen, M., Schonbrunn, E., Biou, V., Thompson, A., Mandelkow, E. M., and Mandelkow, E. (1997) *Cell 91*, 985−994.
17. Sack, S., Muller, J., Marx, A., Thormahlen, M., Mandelkow, E. M., Brady, S. T., and Mandelkow, E. (1997) *Biochemistry 36*, 16155−16165.
18. Kull, F. J., Sablin, E. P., Lau, R., Fletterick, R. J., and Vale, R. D. (1996) *Nature 380*, 550−555.
19. Sablin, E. P., Kull, F. J., Cooke, R., Vale, R. D., and Fletterick, R. J. (1996) *Nature 380*, 555−559.
20. Sablin, E. P., Case, R. B., Dai, S. C., Hart, C. L., Ruby, A., Vale, R. D., and Fletterick, R. J. (1998) *Nature 395*, 813−816.
21. Gulick, A. M., Song, H., Endow, S. A., and Rayment, I. (1998) *Biochemistry 37*, 1769−1776.
22. Turner, J., Anderson, R., Guo, J., Beraud, C., Fletterick, R., and Sakowicz, R. (2001) *J. Biol. Chem. 276*, 25496−25502.
23. Furch, M., Fujita-Becker, S., Geeves, M. A., Holmes, K. C., and Manstein, D. J. (1999) *J. Mol. Biol. 290*, 797−809.
24. Schliwa, M., and Woehlke, G. (2001) *Nature 411*, 424−425.
25. Sack, S., Kull, F. J., and Mandelkow, E. (1999) *Eur. J. Biochem. 262*, 1−11.
26. Kull, F. J., and Endow, S. A. (2002) *J. Cell Sci. 115*, 15−23.
27. Sablin, E. P., and Fletterick, R. J. (2001) *Curr. Opin. Struct. Biol. 11*, 716−724.
28. Case, R. B., Pierce, D. W., Hom-Booher, N., Hart, C. L., and Vale, R. D. (1997) *Cell 90*, 959−966.

29. Endow, S. A., and Waligora, K. W. (1998) *Science 281*, 1200−1202.
30. Henningsen, U., and Schliwa, M. (1997) *Nature 389*, 93−96.
31. Rice, S., Lin, A. W., Safer, D., Hart, C. L., Naber, N., Carragher, B. O., Cain, S. M., Pechatnikova, E., Wilson-Kubalek, E. M., Whittaker, M., Pate, E., Cooke, R., Taylor, E. W., Milligan, R. A., and Vale, R. D. (1999) *Nature 402*, 778−784.
32. Hirose, K., Lowe, J., Alonso, M., Cross, R. A., and Amos, L. A. (1999) *Mol. Biol. Cell 10*, 2063−2074.
33. Hoenger, A., Doerhoefer, M., Woehlke, G., Tittmann, P., Gross, H., Song, Y. H., and Mandelkow, E. (2000) *Biol. Chem. 381*, 1001−1011.
34. Hoenger, A., Sack, S., Thormahlen, M., Marx, A., Muller, J., Gross, H., and Mandelkow, E. (1998) *J. Cell Biol. 141*, 419−430.
35. Hoenger, A., Thormahlen, M., Diaz-Avalos, R., Doerhoefer, M., Goldie, K. N., Muller, J., and Mandelkow, E. (2000) *J. Mol. Biol. 297*, 1087−1103.
36. Sosa, H., Dias, D. P., Hoenger, A., Whittaker, M., Wilson-Kubalek, E., Sablin, E., Fletterick, R. J., Vale, R. D., and Milligan, R. A. (1997) *Cell 90*, 217−224.
37. Wendt, T. G., Volkmann, N., Skiniotis, G., Goldie, K. N., Muller, J., Mandelkow, E., and Hoenger, A. (2002) *EMBO J. 21*, 5969−5978.
38. Tomishige, M., and Vale, R. D. (2000) *J. Cell Biol. 151*, 1081−1092.
39. Xing, J., Wriggers, W., Jefferson, G. M., Stein, R., Cheung, H. C., and Rosenfeld, S. S. (2000) *J. Biol. Chem. 275*, 35413−35423.
40. Rosenfeld, S. S., Jefferson, G. M., and King, P. H. (2001) *J. Biol. Chem. 276*, 40167−40174.
41. Schnitzer M. J., Visscher K., and Block, S. (2000) *Nat. Cell Biol. 2*, 718−723.
42. Sindelar, C. V., Budny, M. J., Rice, S., Naber, N., Fletterick, R., and Cooke, R. (2002) *Nat. Struct. Biol*., 844−848.
43. Farrell, C. M., Mackey, A. T., Klumpp, L. M., and Gilbert, S. P. (2002) *J. Biol. Chem. 277*, 17079−17087.
44. Brendza, K. M., Rose, D. J., Gilbert, S. P., and Saxton, W. M. (1999) *J. Biol. Chem. 274*, 31506−31514.
45. Gilbert, S. P., and Johnson, K. A. (1993) *Biochemistry 32*, 4677−4684.
46. Correia, J. J., Gilbert, S. P., Moyer, M. L., and Johnson, K. A. (1995) *Biochemistry 34*, 4898−4907.
47. Gilbert, S. P., and Johnson, K. A. (1994) *Biochemistry 33*, 1951−1960.
48. Brendza, K. M., Sontag, C. A., Saxton, W. M., and Gilbert, S. P. (2000) *J. Biol. Chem. 275*, 22187−22195.
49. Gilbert, S. P., and Mackey, A. T. (2000) *Methods 22*, 337−354.
50. Nogales, E., Wolf, S. G., and Downing, K. H. (1998) *Nature 391*, 199−203.
51. Jones, T. A., Zou, J. Y., Cowan, S. W., and Kjeldgaard (1991) *Acta Crystallogr. A47* (Part 2), 110−119.
52. Esnouf, R. M. (1997) *J. Mol. Graphics Modell. 15*, 132−133.
53. Woehlke, G., Ruby, A. K., Hart, C. L., Ly, B., Hom-Booher, N., and Vale, R. D. (1997) *Cell 90*, 207−216.
54. Harrison, B. C., Marchese-Ragona, S. P., Gilbert, S. P., Cheng, N., Steven, A. C., and Johnson, K. A. (1993) *Nature 362*, 73−75.
55. Rosenfeld, S. S., Correia, J. J., Xing, J., Rener, B., and Cheung, H. C. (1996) *J. Biol. Chem. 271*, 30212−30221.
56. Hua, W., Chung, J., and Gelles, J. (2002) *Science 295*, 844−888.

BI026715R